

# Quasiparticle Spectrum of $d$ -wave Superconductors in the Mixed State: a Large Fermi-velocity Anisotropy Study

Luca Marinelli and B. I. Halperin

*Physics Department, Harvard University, Cambridge, MA 02138*

(August 21, 2001)

The quasiparticle spectrum of a two-dimensional  $d$ -wave superconductor in the mixed state,  $H_{c1} \ll H \ll H_{c2}$ , is studied for large values of the “anisotropy ratio”  $\alpha_D = v_F/v_\Delta$ . For a square vortex lattice rotated by  $45^\circ$  from the quasiparticle anisotropy axes (and the usual choice of Franz–Tešanović singular gauge transformation) we determine essential features of the band structure asymptotically for large  $\alpha_D$ , using an effective one-dimensional model, and compare them to numerical calculations. We find that several features of the band structure decay to zero exponentially fast for large  $\alpha_D$ . Using a different choice of singular gauge transformation, we obtain a different band structure, but still find qualitative agreement between the 1D and full 2D calculations. Finally, we distort the square lattice into a non-Bravais lattice. Both the one- and two-dimensional numerical calculations of the energy spectra show a gap around zero-energy, with our gauge choice, and the two excitation spectra agree reasonably well.

## I. INTRODUCTION

The quasiparticle spectrum of  $d$ -wave superconductors in the mixed state,  $H_{c1} \ll H \ll H_{c2}$ , has been the object of recent detailed studies. High- $T_c$  superconductors are extreme Type-II superconductors and in a magnetic field  $H \gg H_{c1}$  develop a vortex lattice, the geometry of which depends somewhat on the strength of the magnetic field. The  $d$ -wave symmetry implies the existence of four points on the zero-field Fermi surface where the gap vanishes. This fact has important implications for the low-temperature thermodynamics of these systems, as there are states available even at very low temperatures.

The main questions that have been addressed in the literature are the fate of these gapless points in a finite magnetic field and, more generally, the nature of low-energy states of the quasiparticle spectrum. The standard approach to studying the quasiparticle spectrum in a superconductor is through the Bogoliubov–de Gennes equation<sup>1</sup>, which allows for a spatially varying order parameter in a natural way. Gor’kov and Schrieffer<sup>2</sup> and, in a more recent paper, Anderson<sup>3</sup> neglected in a first approximation the spatially dependent superfluid velocity in the vortex lattice. They predicted that the quasiparticle spectrum in a magnetic field  $H \ll H_{c2}$  is characterized by broadened Landau levels. However, their key assumption, namely treating the superfluid velocity in perturbation theory, is questionable as work by Mel’nikov<sup>4</sup> shows that this singular perturbation strongly mixes Landau levels.

A new approach to tackle these questions was pioneered by Franz and Tešanović<sup>5</sup>. They introduced a singular gauge transformation that takes into account the supercurrent distribution and the magnetic field on an equal footing. Starting from the linearized Bogoliubov–

de Gennes equation<sup>6</sup> in a magnetic field, they mapped the original problem onto one of diagonalizing a Dirac Hamiltonian in an effective periodic vector and scalar potential with vanishing magnetic flux in the unit cell. The new Hamiltonian is more suited to numerical diagonalization, using standard band structure calculation techniques. Within their model, Franz and Tešanović found that the low-energy quasiparticle spectrum stays gapless at the center of the Brillouin zone ( $\Gamma$  point), even in the presence of a magnetic field. They also noticed that, for large anisotropy ratio  $\alpha_D = v_F/v_\Delta$  (where  $v_\Delta = \Delta_0/p_F$  is the quasiparticle velocity parallel to the Fermi surface and  $\Delta_0$  is the maximum magnitude of the bulk zero-field gap function), more low-energy states arise. For larger values of  $\alpha_D$ , they found entire lines in the Brillouin zone where the energies appeared to vanish, within the uncertainty of their numerical calculations.

Because it is difficult to decide by direct numerical calculations whether there are actual zeroes of the dispersion relations, we undertook in a previous paper<sup>7</sup> to employ symmetry considerations, as well as a perturbative analysis and alternative calculational methods to elucidate the properties of solutions of the Franz–Tešanović (FT) equations. The present work continues these efforts by analysing a one-dimensional variant of the FT model, which was also considered by Knapp, Kallin and Berlinsky<sup>8</sup>.

The one-dimensional model has the advantage that it can be solved numerically or analytically with arbitrary accuracy, and its asymptotic behavior, for large values of  $\alpha_D$  can be readily extracted. Moreover, the behavior of the 1D model and the two-dimensional FT model are very close to each other for large values of the anisotropy ratio  $\alpha_D$ . Thus we can gain valuable insight into the solutions of these equations.

We note that relatively large values of the anisotropy ratio are relevant to actual high- $T_C$  superconductors,

namely  $\alpha_D$  ranging between 10 and 20. (From angle-resolved photoemission spectroscopy and thermal conductivity measurements, the value of  $\alpha_D$  for high- $T_c$  superconductors turns out to be about 14 for YBCO<sup>9</sup> and 20 for Bi2212<sup>9,10</sup>.)

The singular gauge transformation introduced by Franz and Tešanović is exact in the region of space outside the vortex core where the magnitude of the gap parameter  $|\Delta(\mathbf{r})|$  is independent of position. As we are interested in the situation of weak magnetic fields, where the vortex cores occupy a very small fraction of the total area, it is natural to suppose that errors in the energies introduced by an arbitrary treatment of the core interior would not be significant. However, the situation is more subtle, as was noted by Vafeek, Melikyan and Tešanović<sup>11</sup>.

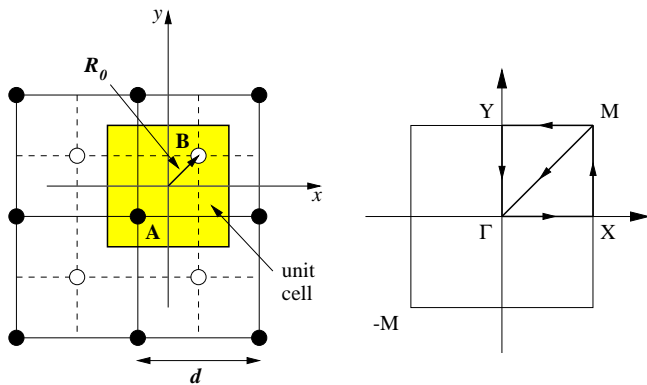


FIG. 1. (a) A and B sublattices and vortex lattice unit cell. (b) The corresponding magnetic Brillouin zone.

The energy states of interest have a large weight in the vicinity of the vortex cores, and the energies can be shifted by amounts which are finite on the scale of  $E_1 = \hbar v_F/d$  ( $d$  is the distance between nearest vortices belonging to the same FT sublattice, as defined in Fig. 1), depending on what one assumes for the behavior inside the vortex core. Alternatively, one can introduce a mathematical boundary condition at the radius of the vortex core. The wavefunction, which obeys the FT equations outside the core, must satisfy appropriate boundary conditions at the boundary of the core. It appears, however, that there are a variety of possible boundary conditions which remain mathematically sensible and distinct in the limit of vanishing core radius. An analysis of the behavior inside the core is therefore ultimately necessary to find the behavior appropriate to a given microscopic Hamiltonian or for an actual high- $T_C$  superconductor, even in the limit of weak magnetic fields.

We do not address this problem here. Instead, we follow the approach of Franz and Tešanović<sup>5</sup> and our own subsequent work<sup>7</sup>, in which, for a given choice of the singular gauge transformation, the vortex core is treated by smoothing the superfluid velocities over a small area. Although this approach appears to be well defined in the limit where the core-radius vanishes relative to the vortex

separation, the energy spectrum obtained does depend on the particular choice made in the FT gauge transformation. (*i.e.*, the energy spectrum depends on which vortices are assigned to each of the two FT sublattices.) Similarly, each of the one-dimensional models considered in the present paper depend on the choice of FT gauge used in the 2D model from which it was derived, and the resulting dispersion relations reflect the differences between the parent 2D models.

The essence of the one-dimensional model is to smear the vortices in the  $y$  direction (as defined in Fig. 1). This direction is the “hard” direction, meaning that wavefunctions in this direction change very slowly. In particular, if we focus on the low-energy states, any fluctuation of the quasiparticle wavefunctions in the  $y$  direction (for large anisotropy) will be energetically very costly. For this reason, it is reasonable to assume that asymptotically for  $\alpha_D \rightarrow \infty$  the lowest-energy states will be translationally invariant in the  $y$  direction (and, more generally, they will be represented by plane waves in the  $y$  direction with a wavevector  $k_y$  equal to a reciprocal vector of the vortex lattice, if higher energy states are to be taken into account). Of course, this assumption depends crucially on the orientation of the vortex lattice with respect to the quasiparticle anisotropy axes. We consider a square vortex lattice tilted by  $45^\circ$  with respect to the anisotropy axes. If the angle was different, a line going through a vortex along the “hard” direction would not necessarily intersect other vortices (incommensurate case) or could intersect another vortex some number of unit cells away from the vortex we considered (commensurate case). In either case the description would be more complicated than the one considered here.

Mel’nikov<sup>4</sup> was the first to realize that the Bogoliubov–de Gennes equation for a  $d$ -wave superconductor in the mixed state is simplified in the large anisotropy limit  $\alpha_D \gg 1$ . He derived a one-dimensional approximate model and described how to solve it, although he confined his analysis to the semiclassical version of these solutions. Knapp, Kallin and Berlinsky<sup>8</sup>, starting from the FT equations, derived a 1D model valid for large  $\alpha_D$  and carried out a fully quantum mechanical calculation of the properties of this model. They worked in the singular gauge introduced by Franz and Tešanović<sup>5</sup> matched the solutions in terms of parabolic cylinder functions at the boundaries of the unit cell to obtain an exact excitation spectrum for the one-dimensional Hamiltonian. This matching, although exact, was nevertheless carried out numerically and therefore did not give analytical information on the dependence of the features of the band structure on the anisotropy  $\alpha_D$ .

We have found that the most important features of the one-dimensional model can be understood and calculated using an approach which emphasizes the underlying physics in a more transparent way. In essence, the low-energy states are localized around one of the two vortices in the unit cell and, in the large anisotropy limit, the overlap between linearly independent wavefunctions

can become exponentially small as a function of  $\alpha_D$  if the potential wells these states are confined in are spatially separated. In the singular FT gauges that exhibit this exponential behavior, features of the energy bands, such as the minimum energy in the  $\Gamma Y$  direction (away from the  $\Gamma$  point) or the bandwidth of the  $\Gamma X$  lowest energy band, can be calculated analytically in the WKB approximation.

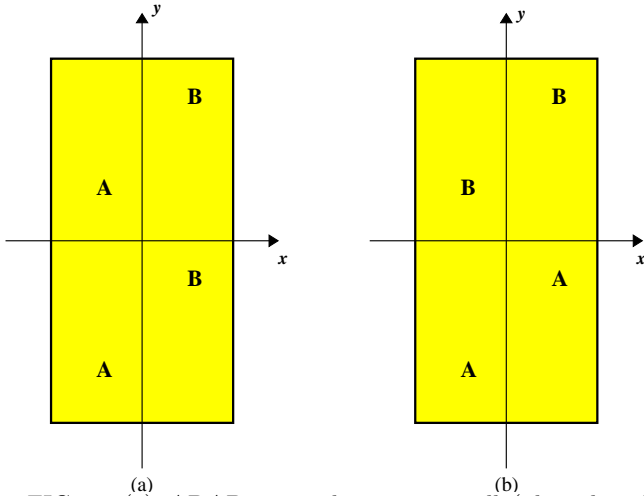


FIG. 2. (a) *ABAB* vortex lattice unit cell (plotted with four vortices per unit cell). (b) *AABB* vortex lattice unit cell.

The lower dimensionality of the model under study in this paper, allows also for much smaller scale numerical calculations to find the quasiparticle spectrum than the two-dimensional case, as was already pointed out by Knapp, Kallin and Berlinsky<sup>8</sup>. Some of the features which were hard to resolve in the full two-dimensional problem, such as the band structure along the  $\Gamma X$  symmetry line and the apparent lines of zero-energy states that formed parallel to the  $\Gamma X$  line and intersected the  $\Gamma Y$  line at non-symmetry points, become readily accessible in the one-dimensional model. In this work we have performed such numerical calculations for two different singular gauge choices and found good agreement with the asymptotic analysis and the data available for the two-dimensional model in both cases. In the first singular gauge, which we called *ABAB* following Vafeek *et al.*<sup>12</sup> (see Fig. 2), the low-energy features of the spectrum exhibit the above-mentioned exponential dependence on  $\alpha_D$ , while in the second gauge, which we called *AABB*, they do not.

If, after including the appropriate vortex core physics, the correct energy spectrum in the continuum limit turns out to be related to the results in the *ABAB* gauge, we could use the above results to improve our understanding of the relation between the semiclassical description of the quasiparticle spectrum in the vortex state, as derived by Volovik<sup>13</sup> and the fully quantum-mechanical picture. The semiclassical density of states is characterized by two crossover energy scales,  $E_1$  and  $E_2$  ( $E_2 < E_1$ ).

For energies  $E \gg E_1 = \hbar v_F/d$  the density of states is, on average, quantitatively identical to that in the absence of a magnetic field, while for  $E < E_1$  the density of states can be evaluated in a semiclassical approximation and turns out to be constant. The semiclassical description breaks down at the energy scale  $E_2$ , where a full quantum mechanical calculation becomes necessary. In our previous paper<sup>7</sup>, we noticed that the value of the crossover energy scale  $E_2$  predicted by Kopnin and Volovik<sup>14–16</sup>  $E_2^{KV} \approx \hbar v_\Delta/d$  did not seem to match with our numerical findings, at least for the vortex lattice geometries we considered. In fact, it seemed that  $E_2$  went to zero much faster than linearly in  $1/\alpha_D$ . Furthermore, recent specific heat<sup>17</sup> and low temperature thermal conductivity<sup>18</sup> experiments have been performed in the regime  $E < E_2^{KV}$  and still show good agreement with the semiclassical predictions, which seems to suggest that the correct crossover scale between the quantum mechanical and semiclassical regimes is much smaller than  $E_2^{KV}$ , for large anisotropy ratios. The one-dimensional model provides the key to this puzzle, as both the bandwidth of the lowest  $\Gamma X$  energy band and the minima of the  $\Gamma Y$  band (away from the  $\Gamma$  point) are shown to be suppressed exponentially for large  $\alpha_D$ , instead of linearly. In particular, the larger of these two energies will determine the crossover between the semiclassical and quantum mechanical regimes, where the details of the band structure become important to determine the density of states.

We also studied the one-dimensional energy spectrum of a non-Bravais vortex lattice, with the usual choice of singular gauge (*ABAB*). In this case, we previously found<sup>7</sup> that the two-dimensional band structure becomes gapped. It has been suggested recently by Vishwanath<sup>19</sup> that this gap may be a spurious feature of the Franz–Tešanović *ABAB* model; indeed one can make other choices for the singular gauge transformation, assigning the vortices to sublattices in a different way, so that the spectrum is gapless for the very geometry in question. We do not try to answer here the question of whether a gap would be present in this geometry when one treats properly the region inside the vortex cores. We limit ourselves here to the observation that given a particular choice of the singular gauge transformation the spectra of the two-dimensional model and of the one-dimensional model derived from it agree reasonably well at long values of  $\alpha_D$ . In both cases the lowest positive and negative energy bands are separated by a finite energy gap, and the minimum energy separation between the two bands does not occur at the  $\Gamma$  point (for anisotropy  $\alpha_D \neq 1$ ). Similarly to other results discussed in this paper, this energy gap could be a feature which depends on the choice of vortex core physics. Whether it survives or not the correct choice of boundary conditions is not within the scope of this paper. We limit ourselves to note that given a singular gauge transformation, we find good agreement between the spectra of the one- and two-dimensional Hamiltonians.

To summarize the structure of the paper, the one-

dimensional model Hamiltonian is derived in Sec. II. The asymptotic analysis of the band structure for large anisotropy follows in Sec. III. Numerical results can be found in Sec. IV, where a comparison between two different singular gauge choices is shown explicitly, together with a study of the excitation spectrum of a non-Bravais vortex lattice. Conclusions follow in Sec. V. A derivation of the WKB approximation and an account of the numerical methods can be found in Appendix A and B, respectively.

## II. DERIVATION OF THE ONE-DIMENSIONAL MODEL

The properties of the quasiparticle spectrum in a superconductor in an external magnetic field are best studied in the framework of the Bogoliubov–de Gennes equation<sup>1</sup>. To establish notations and for overall clarity, we will very briefly summarize the most important points of the derivation of the Bogoliubov–de Gennes equation for a  $d$ -wave superconductor in the mixed state, more details can be found in our earlier paper<sup>7</sup> (see also<sup>12</sup>).

We will consider the Bogoliubov–de Gennes operator for a  $d_{xy}$ -superconductor instead of the more conventional  $d_{x^2-y^2}$ , purely for notational simplicity; results do not depend on this choice. Also, because we are only interested in the low-energy properties of the spectrum and because we consider magnetic fields  $H \ll H_{c2}$  (i.e. such that the size of the vortex lattice unit cell is much larger than  $1/k_F$ ), we can linearize the Bogoliubov–de Gennes equation around one of the four gapless points on the Fermi surface. Choosing  $\mathbf{p} = (0, p_F)$ , the linearized Bogoliubov–de Gennes operator reads<sup>6</sup>

$$\tilde{\mathcal{H}}_{\text{lin}} = \begin{pmatrix} v_F(p_y - \frac{e}{c}A_y) & \frac{1}{p_F}\{p_x, \Delta(\mathbf{r})\} \\ \frac{1}{p_F}\{p_x, \Delta^*(\mathbf{r})\} & -v_F(p_y + \frac{e}{c}A_y) \end{pmatrix}, \quad (1)$$

where  $\Delta(\mathbf{r}) = \Delta_0 e^{i\phi(\mathbf{r})}$  is the Ginzburg–Landau order parameter and the brackets represent symmetrization  $\{a, b\} = \frac{1}{2}(ab + ba)$ .

In the singular gauge introduced by Franz and Tešanović<sup>5</sup>, we can eliminate the position dependent phase factor  $e^{i\phi(\mathbf{r})}$  from the off-diagonal components of the Bogoliubov–de Gennes equation (1). The resulting Bogoliubov–de Gennes operator after the gauge transformation is

$$\mathcal{H}_{\text{lin}} = \begin{pmatrix} v_F p_y & v_\Delta p_x \\ v_\Delta p_x & -v_F p_y \end{pmatrix} + m \begin{pmatrix} v_F v_{sy}^A & \frac{v_\Delta}{2}(v_{sx}^A - v_{sx}^B) \\ \frac{v_\Delta}{2}(v_{sx}^A - v_{sx}^B) & v_F v_{sy}^B \end{pmatrix}, \quad (2)$$

$$\mathcal{H} = \begin{pmatrix} \frac{1}{i} \partial_y + U_y^A & \frac{1}{i\alpha_D} \partial_x + \frac{1}{2\alpha_D} (U_x^A - U_x^B) \\ \frac{1}{i\alpha_D} \partial_x + \frac{1}{2\alpha_D} (U_x^A - U_x^B) & -\frac{1}{i} \partial_y + U_y^B \end{pmatrix}. \quad (5)$$

where  $v_\Delta = \Delta_0/p_F$ . The superfluid velocities corresponding to the  $A$  and  $B$  sublattices of the vortex lattice, as defined in Fig. 1, are

$$\mathbf{v}_s^\mu = \frac{1}{m}(\hbar \nabla \phi_\mu - \frac{e}{c} \mathbf{A}), \quad \mu = A, B \quad (3)$$

where  $\phi(\mathbf{r}) = \phi_A(\mathbf{r}) + \phi_B(\mathbf{r})$ . The operator (2) describes the dynamics of a non-interacting Dirac particle in a periodic scalar and vector potential and general features of its spectrum have been studied in detail elsewhere<sup>5,7,12</sup>.

The Bogoliubov–de Gennes equation should in principle be solved self-consistently, thus finding the order parameter distribution (from which the geometry of the minimum free-energy vortex lattice configuration can be inferred) together with the energies and wavefunctions of the quasiparticle excitations. At low temperatures and for the magnetic field range considered here, to a good approximation, the order parameter distribution can be computed in Ginzburg–Landau theory and substituted in the Bogoliubov–de Gennes equation, without iterating it to achieve self-consistency. We studied the quasiparticle spectrum in this approximation, choosing a square vortex lattice rotated by  $45^\circ$  from the quasiparticle anisotropy axes.

In this work we want to focus on the large anisotropy  $\alpha_D = v_F/v_\Delta \gg 1$  limit. For this reason we have decided to study a one-dimensional model which captures the essential physics of the large-anisotropy regime and we believe becomes asymptotically exact in the  $\alpha_D \rightarrow \infty$  and low-energy limit. The essence of the model is to smear out the vortices in the  $y$  direction (the “hard” direction). The absolute value of the low-energy two-dimensional wavefunctions has only small ripples and overall fluctuations in the “hard” direction, thus motivating the claim that asymptotically the low-energy eigenstates of (2) should factor into a plane wave in the  $y$  direction times a Bloch state in the  $x$  direction.

To simplify equations we will write lengths in units of the distance between nearest-neighbor vortices  $d$  and energies in units of  $E_1 = \hbar v_F/d$ . Let us define the dimensionless periodic potentials

$$U_{x,y}^{A,B} = \frac{md}{\hbar} v_{sx,y}^{A,B} = \partial_{x,y} \phi^{A,B} - \frac{ed}{\hbar c} A_{x,y} \quad (4)$$

where the vector potential is chosen to satisfy the Landau gauge  $A_x = -dB_y$  and  $A_y = 0$ . The Bogoliubov–de Gennes operator can then be rewritten in dimensionless form

The one-dimensional approximation amounts to assuming that gauge invariant quantities can only be a function of  $x$ . In particular, the potentials  $U_y^{A,B}$  and  $U_x^{A,B}$  are gauge invariant quantities and thus

$$\partial_y (\partial_x \phi^{A,B} + 2\pi y) = 0 \quad (6)$$

which, away from the vortices, implies

$$\partial_y \phi^{A,B} = -2\pi x + \text{const.} \quad (7)$$

The constant of integration in the above expression changes discontinuously when crossing a line of vortices and can be determined by imposing that the potentials  $U_y^{A,B}$  are periodic (with period 1) and have zero average and that

$$\oint_C \nabla \phi^{A,B} \cdot d\mathbf{l} = 2\pi N_{A,B}, \quad (8)$$

where  $N_{A,B}$  is the number of  $A$  or  $B$  vortices in the unit cell. The path  $C$  is a rectangle enclosing a line of vortices with infinitesimal width in the  $x$  direction and spanning the vortex lattice unit cell in the  $y$  direction. Furthermore, in the large-anisotropy limit,  $v_{sx}^A$  and  $v_{sx}^B$  will both vanish. The periodicity of the potentials can be used to further simplify the calculation by writing the wavefunctions in Bloch form

$$\begin{pmatrix} v_{\mathbf{k}}(x, y) \\ w_{\mathbf{k}}(x, y) \end{pmatrix} = e^{i(k_x x + k_y y)} \begin{pmatrix} V_{\mathbf{k}}(x) \\ W_{\mathbf{k}}(x) \end{pmatrix}. \quad (9)$$

The final result is that the one-dimensional effective Hamiltonian acting on Bloch states takes the form

$$\mathcal{H}_{1D} = \begin{pmatrix} k_y + U^A(x) & \frac{1}{i\alpha_D} \partial_x + \frac{1}{\alpha_D} k_x \\ \frac{1}{i\alpha_D} \partial_x + \frac{1}{\alpha_D} k_x & -k_y + U^B(x) \end{pmatrix}. \quad (10)$$

We have considered three different vortex arrangements, two of which represent the same physical situation of a square Bravais lattice of vortices and one is an inversion-symmetric non-Bravais lattice. The two Bravais vortex lattices differ in the labeling of the vortices, as can be seen in Fig. 2. Following Vafeek *et al.*<sup>12</sup>, we will refer to them as the *ABAB* and *AABB* configuration, respectively.

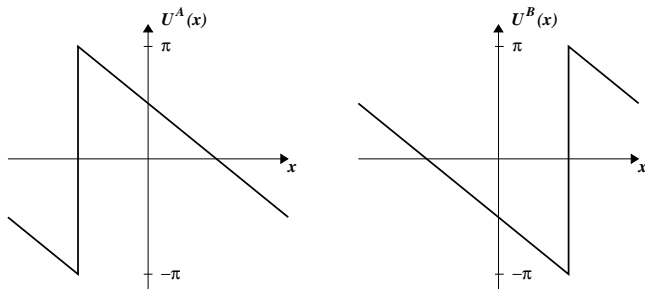


FIG. 3. The one-dimensional periodic potentials  $U^A(x)$  and  $U^B(x)$  in the *ABAB* gauge are plotted in the unit cell. Energies are in units of  $\hbar v_F/d$ .

In the *ABAB* case, we can work with a unit cell with one  $A$  and one  $B$  vortex. In this case the potentials  $U^A(x)$  and  $U^B(x)$  can be calculated as outlined above to find

$$U^A(x) = \begin{cases} -2\pi x - \frac{3}{2}\pi, & -\frac{1}{2} \leq x \leq -\frac{1}{4} \\ -2\pi x + \frac{1}{2}\pi, & -\frac{1}{4} < x \leq \frac{1}{2} \end{cases} \quad (11)$$

and

$$U^B(x) = \begin{cases} -2\pi x - \frac{1}{2}\pi, & -\frac{1}{2} \leq x \leq \frac{1}{4} \\ -2\pi x + \frac{3}{2}\pi, & \frac{1}{4} < x \leq \frac{1}{2}. \end{cases} \quad (12)$$

The  $U^A(x)$  and  $U^B(x)$  potentials in the *ABAB* gauge are plotted in Fig. 3.

Alternatively, we considered the *AABB* configuration, in which case one has to work with a unit cell containing four vortices (two of type  $A$  and two of type  $B$ ). In this case the discontinuity of the potentials across a line of vortices is  $\pi$  (this should be compared to  $2\pi$  in the case of the *ABAB* lattice) and the  $U^A(x)$  and  $U^B(x)$  potentials are identical across the unit cell

$$U^A(x) = U^B(x) = \begin{cases} -2\pi x - \pi, & -\frac{1}{2} \leq x \leq -\frac{1}{4} \\ -2\pi x, & -\frac{1}{4} \leq x \leq \frac{1}{4} \\ -2\pi x + \pi, & \frac{1}{4} \leq x \leq \frac{1}{2}. \end{cases} \quad (13)$$

The one-dimensional model can be derived also for a class of non-Bravais lattices. In particular, we studied an inversion-symmetric lattice, whose quasiparticle spectrum we analyzed in detail in a previous paper<sup>7</sup>. This lattice has two vortices per unit cell whose distance along the diagonal,  $2R_0$  (see Fig. 1), is different from  $(\sqrt{2}/2)d$  (which corresponds to evenly spaced  $A$  and  $B$  vortices, necessary condition for a Bravais lattice). For concreteness, let us consider the case where the two sublattices  $A$  and  $B$  are still square lattices with spacing  $d$ , but the distance between nearest  $A$  and  $B$  vortices is now  $(2x_v\sqrt{2})d$ . Switching back to dimensionless units, the  $A$  and  $B$  vortices in the unit cell are located at coordinates  $(-x_v, -x_v)$  and  $(x_v, x_v)$  respectively, instead of  $(\pm 1/4, \pm 1/4)$ , as in the Bravais lattice case. Here we are particularly interested in determining whether the appearance of a gap in the excitation spectrum (as was found before in the two-dimensional numerical analysis) is peculiar to the two-dimensional model or is a feature of the one-dimensional approximation as well. To this end, we have calculated the  $U^A(x)$  and  $U^B(x)$  potentials when the lines of vortices are located at  $x = \pm x_v$

$$U^A(x) = \begin{cases} -2\pi x - (2x_v + 1)\pi, & -\frac{1}{2} \leq x \leq -x_v \\ -2\pi x - (2x_v - 1)\pi, & -x_v < x \leq \frac{1}{2} \end{cases} \quad (14)$$

and

$$U^B(x) = \begin{cases} -2\pi x + (2x_v - 1)\pi, & -\frac{1}{2} \leq x \leq x_v \\ -2\pi x + (2x_v + 1)\pi, & x_v < x \leq \frac{1}{2}. \end{cases} \quad (15)$$

Note that the discontinuity of the  $U^A(x)$  and  $U^B(x)$  potentials at the vortex lines is always  $2\pi$ , regardless of the

location of the vortices. These potentials will be used in the analysis of the excitation spectrum, both in numerical calculations and in the asymptotic analysis of prominent features of the band structure for the *ABAB* vortex lattice.

### III. ASYMPTOTIC ANALYSIS OF THE BAND STRUCTURE FOR THE *ABAB* VORTEX LATTICE

The one-dimensional model can be solved exactly by matching the parabolic cylinder function solutions<sup>4</sup> across the boundary of the unit cell. This method requires a numerical exact calculation to match the boundary conditions and leads to results which are practically indistinguishable from the numerical diagonalization of the one-dimensional model, as shown by Knapp, Kallin and Berlinsky<sup>8</sup>. Here we use an alternative approach which does not provide an analytical solution of the one-dimensional model for arbitrary values of the anisotropy but it allows us to understand in a relatively simple way the leading behavior of the quasiparticle spectrum for large values of the anisotropy ratio  $\alpha_D$ . In this section we will limit our analysis to the *ABAB* vortex lattice, although we will comment on the other gauge choice that was introduced in the previous section.

In essence, in the large anisotropy limit and for the *ABAB* configuration, the low-energy wavefunctions are localized in the triangular potential wells  $U^A(x) + k_y$  and  $U^B(x) - k_y$ , defined in equation (10) with the potentials (12). The tails of these wavefunctions overlap in the classically forbidden regions of the potential wells, and the overlap becomes exponentially small for large  $\alpha_D$ . Using  $1/\alpha_D$  as our “small” parameter, we can develop a WKB approach which can be used to calculate the leading exponential dependence on  $\alpha_D$  of the tails of the wavefunctions. This, in turn, allows us to understand the features of the band structure, like the lowest energy band widths and energy splittings at near crossings.

There are a number of consequences of the small overlap between wavefunctions localized around different vortices, as the anisotropy  $\alpha_D$  grows larger. First of all, note that the one-dimensional Hamiltonian (10) can be split in the following way

$$\mathcal{H}_{1D} = \mathcal{H}_0 + k_y \sigma_3 \quad (16)$$

where  $\mathcal{H}_0$ , the one-dimensional Hamiltonian computed at  $k_y = 0$ , is independent of  $k_y$  and  $\sigma_3$  is the diagonal Pauli spin matrix. This implies that the expectation value of  $\mathcal{H}_{1D}$  in the state  $\psi(x)$ ,  $\mathcal{E} = \langle \mathcal{H}_{1D} \rangle_\psi$ , obeys

$$\frac{\partial \mathcal{E}}{\partial k_y} = \langle \sigma_3 \rangle_\psi. \quad (17)$$

If the wavefunction  $\psi(x)$  is localized entirely around the left (respectively right) vortex in the unit cell, its only

non-zero component will be the upper (resp. lower) one. In this case,  $\langle \sigma_3 \rangle_\psi = +1$  (resp.  $-1$ ), and the slope of the energy bands is fixed, regardless of the value of  $\alpha_D$ . This is the case for lowest energy eigenstates close to the Y point, especially at large anisotropy, as the potentials that go into the one-dimensional Hamiltonian (10) correspond to a roughly triangular well for one component, with the bottom of the well close to the energy eigenvalue, and an almost constant potential for the other component, with a fairly large energy difference between the constant potential and the low-energy eigenvalue. In this approximation, the low-energy eigenstates of  $\mathcal{H}_{1D}$  are Airy functions, for one component, and zero for the other. In the repeated band scheme, we expect the band structure close to the Y point to look like parallel lines, the positive energy ones with slope  $+1$ , and the negative energy ones with slope  $-1$  (the negative slope curves with positive energy in Fig. 4 correspond to values of  $-\pi \leq k_y \leq -\pi$ , in the extended zone scheme). This is because around  $k_y = \pi$ , the potential  $U^A(x) + k_y$  is pushed up in energy, while  $U^B(x) - k_y$  is pushed down, and therefore, in the limit  $\alpha_D \rightarrow \infty$ , the positive energy states are strongly localized around the left vortex in the unit cell, while the negative energy states are localized around the right hand one.

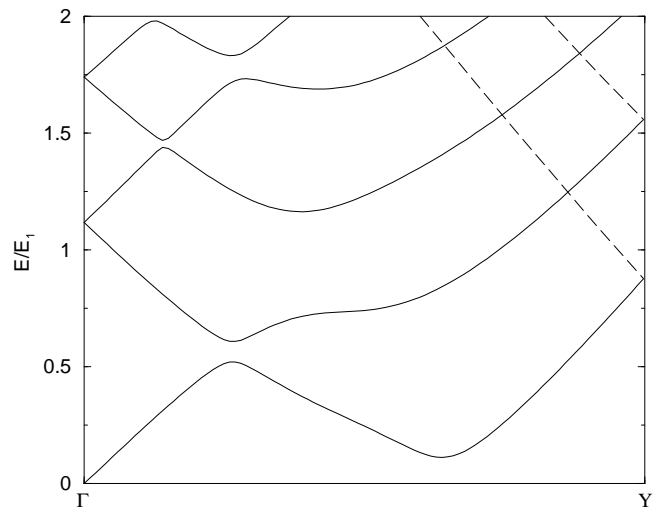


FIG. 4. Band structure of the one-dimensional model in the *ABAB* gauge for a square lattice with anisotropy  $\alpha_D = v_F/v_\Delta = 12$  along the  $\Gamma Y$  direction. The two branches of each band correspond to  $0 \leq k_y \leq \pi$  (solid curves) and  $-2\pi \leq k_y \leq -\pi$  (dashed curves). Only positive energy bands are plotted for clarity, negative energy bands can be obtained through particle-hole symmetry. Energies are in units of  $E_1 = \hbar v_F/d$ .

Let us turn our attention to the first near crossing at approximately zero energy along the  $\Gamma Y$  line, closest to the Y point. We claim that the energy splitting between the first positive and negative energy bands is exponentially small in the anisotropy  $\alpha_D$ . We want to calculate the leading behavior of this splitting for large  $\alpha_D$ , there-

fore we will work in the WKB approximation. The leading exponential expression of the WKB wavefunctions corresponding to energy  $E$  takes the form

$$u(x) \sim e^{\pm\alpha_D \int^x \sqrt{-(E-k_y-U^A(x))(E+k_y-U^B(x))}} \quad (18)$$

and analogously for the lower component  $v(x)$ , as dis-

$$\int_{x_-^E}^{x_+^E} dx \sqrt{\left(E + 2\pi x + \frac{\pi}{2}\right) \left(E + 2\pi x + \frac{3}{2}\pi\right)} = \frac{\pi}{\alpha_D} \left(n - \frac{1}{4}\right), \quad (19)$$

with  $n \geq 1$ . On the right hand side we have used the connection rules for a soft boundary on one side and a hard boundary on the other side of the classically allowed region, as we assumed that the energy of the eigenstate is small compared to the height of the triangular well. The integral on the left hand side of equation (19) can be evaluated explicitly to find

$$\frac{1}{\pi} \left(E + \frac{\pi}{2}\right) \sqrt{E(E + \pi)} - \frac{\pi}{8} \sinh^{-1} \sqrt{\frac{E}{\pi}} \sim \frac{1}{3\sqrt{\pi}} E^{3/2}, \quad (20)$$

where we have used  $\sinh^{-1} x \sim x$  for  $x \ll 1$ . This condition translates in our case to  $E \ll \pi$ , which, for large enough  $\alpha_D$ , is satisfied even for large  $n$ , thereby justifying the usage of the Bohr-Sommerfeld quantization formula. In conclusion, we find the quasiparticle spectrum at the Y point to be

$$E_n \sim \pi \left(\frac{3(n - \frac{1}{4})}{\alpha_D}\right)^{2/3} \quad (21)$$

with  $n = 1, 2, \dots$ . From our previous discussion, we also know that as we go away from the Y point the slope of the energy band is either +1 or -1, depending on their sign. This means that, if we neglect the level repulsion for the moment, the lowest positive and negative energy bands will cross at zero energy (because of the underlying particle-hole symmetry) at  $k_y^* \equiv \pi \left(1 - \left(\frac{9}{4\alpha_D}\right)^{2/3}\right)$ .

$$\begin{aligned} \Delta_{\min} &\sim \exp\left(-\alpha_D \int_{x_R^*}^{x_L^*} dx \sqrt{-\left(-2\pi x - \frac{3}{2}\pi + k_y^*\right) \left(-2\pi x - \frac{1}{2}\pi - k_y^*\right)}\right) \\ &\sim \exp\left[-\frac{\pi^2}{16} \alpha_D \left(1 - 4\left(\frac{9}{4\alpha_D}\right)^{2/3}\right)\right]. \end{aligned} \quad (22)$$

The first minimum away from the  $\Gamma$  point along the  $\Gamma Y$  line develops for  $\alpha_D > 7$ . For larger values of  $\alpha_D$  more minima in the band structure can be found (for example, see Fig. 5), increasing the density of states close to zero energy, and those band gaps can be computed in an analogous fashion to find more exponentially small energy splittings.

Another feature of the band structure that we can un-

derstand in more detail in Appendix A. We can calculate the lowest energy levels at the Y point using the Bohr-Sommerfeld quantization rule. If  $|E| < 2\pi$ , the turning points for the left vortex (centered at  $x = -1/4$ ) are  $x_-^E = -\frac{1}{4} - \frac{E}{2\pi}$  and  $x_+^E = -1/4$ , therefore the quantization condition reads

We can now find the magnitude of the splitting between the lowest positive and negative energy bands at  $k_y^*$ . Our method follows closely the LCAO approximation in molecular physics. We consider two wavefunctions corresponding to the lowest-energy states localized around each vortex for  $k_y = k_y^*$ , that is spinors with either a non-vanishing upper or lower component. If these states were true eigenstates of the one-dimensional Hamiltonian (10), the corresponding eigenvalue would be zero, by definition of  $k_y^*$ . Because the “small” component of the spinor wavefunction is not exactly zero, we can evaluate variationally the exponential dependence of the lowest eigenvalues on the spatial separation of the wavefunctions calculating the overlap integral between the WKB wavefunctions of the two zero-energy states. Because of the periodicity of the potential, there are in principle two regions which are classically forbidden and therefore contribute to the tunneling amplitude between the wavefunction localized around one vortex and the other. On the other hand, for low-energy states, one of these regions (going from one vortex site to the other, regardless of the value of the energy) is wider and the product of the potentials is larger than in the other region, therefore contributing only a subleading exponential behavior. For this reason we will only be concerned with the region between  $x_R^* \equiv -1/4 - k_y^*/(2\pi)$  and  $x_L^* \equiv -3/4 + k_y^*/(2\pi)$  and the overlap integral between the two wavefunctions is

derstand with this simple model is the width of the lowest positive and negative energy bands along the  $\Gamma X$  direction. Once again, to find a variational estimate of this band width, we need to compute the overlap integral between two low-energy wavefunctions. This time, we can start from the two zero-energy states at the  $\Gamma$  point and calculate the  $\Gamma X$  band assuming that it is a narrow tight-binding band arising from the overlap of these two states.

Again, for large  $\alpha_D$ , we expect the width of this band to be exponentially close to zero. The lowest positive and negative energy bands along the  $\Gamma X$  direction in the Brillouin zone can be calculated in the tight-binding approximation

$$\mathcal{E}(k_x) = \pm \Delta E_{\Gamma X} \sin \frac{k_x}{2} \quad (23)$$

where  $\Delta E_{\Gamma X}$  is given by the overlap integral of the two zero-energy wavefunctions. For large  $\alpha_D$ , we can again use the WKB approximation to find the asymptotic leading behavior of the bandwidth

$$\Delta E_{\Gamma X} \sim e^{-\alpha_D \int_{-1/4}^{1/4} dx \sqrt{-U^A(x)U^B(x)}} = e^{-\frac{\pi^2}{16}\alpha_D}. \quad (24)$$

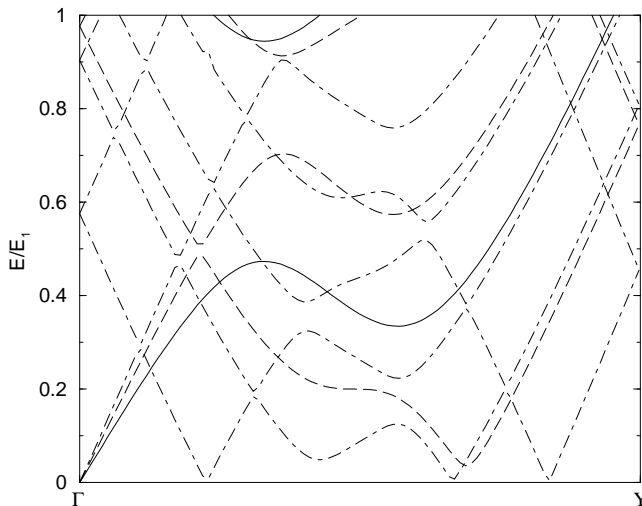


FIG. 5. Band structure of the one-dimensional model in the *ABAB* gauge for a square lattice with anisotropy  $\alpha_D = v_F/v_\Delta = 8, 15, 35$  along the  $\Gamma Y$  direction (solid, dashed and dot-dashed curve respectively). Only positive energy bands are plotted for clarity, negative energy bands can be obtained through particle-hole symmetry. Energies are in units of  $E_1 = \hbar v_F/d$ .

To summarize the asymptotic analysis of the one-dimensional model in the vortex lattice geometry performed in this section, we have explained the parallel energy bands in the  $\Gamma Y$  direction close to the  $\Gamma$  point and their slope. We have also calculated the leading exponential dependence on  $\alpha_D$  of the  $\Gamma X$  bandwidth and of the minima of the  $\Gamma Y$  bands close to zero energy. In the next section, we will describe the numerical solution of the one-dimensional model and compare these analytic results to the numerical data. These results are important to understand the right crossover scale between the quantum mechanical and semiclassical regimes of the density of states, as discussed in the introduction and in our previous publication<sup>7</sup>.

Very different results would be expected in a singular gauge which does not spatially separate the low-energy wavefunctions, for example the *AABB* gauge. As we

showed in the previous section, the potentials  $U^A(x)$  and  $U^B(x)$  in the *AABB* gauge are identical (see eq. (13)), therefore the triangular potential wells corresponding to a line of *A* or *B* vortices are not spatially separated, as in the *ABAB* case, and the wavefunctions localized around the two vortices always have a finite overlap. The nature of the asymptotic limit for large  $\alpha_D$  is then very different from the case discussed above. We do not expect to find an exponential dependence of the features of the energy spectrum on the anisotropy, in either one- or two-dimensions. Numerical calculations confirm this claim, as will be shown in the following section.

## IV. NUMERICAL RESULTS

### A. Bravais vortex lattice: *ABAB* gauge

We have studied the one-dimensional Hamiltonian (10) numerically discretizing it on a real-space grid in one dimension. The reduced dimensionality compared to the Bogoliubov–de Gennes operator (2) allows for much smaller scale numerical calculations and is the key to accessing the large-anisotropy regime. We choose a real-space representation of the one-dimensional model in order to be able to take advantage of sparse matrix diagonalization algorithms (see Appendix B for further details on the numerical methods), although we checked some of our results against a diagonalization of the Hamiltonian (10) in momentum space without finding any appreciable difference. Knapp, Kallin and Berlinsky<sup>8</sup> diagonalized the one-dimensional model in the *ABAB* gauge in momentum space and did not find any appreciable difference from our results in the range of overlap.

Let us start discussing the numerical diagonalization in the case of the *ABAB* singular gauge. From the analytical results discussed in the previous section and our previous numerical investigation of the two-dimensional Bogoliubov–de Gennes equation<sup>7</sup>, we expect to find points in the Brillouin zone where the energy spectrum has an eigenvalue which is exponentially close to zero. The simplicity of the numerical implementation of the one-dimensional model allows us to resolve these eigenvalues in detail and to compare them to our previous results in two dimensions.

Scanning the vortex lattice Brillouin zone we have computed the band structure for several values of the anisotropy ratio  $\alpha_D$ . The quasiparticle bands in a square vortex lattice are symmetric under the exchange of  $k_x \rightarrow -k_x$  or  $k_y \rightarrow -k_y$ , hence only positive  $k_x$  or  $k_y$  have generally been considered. Also, particle-hole symmetry holds at each point in the Brillouin zone, therefore only positive energies need to be taken into account. In the one-dimensional model, the potentials  $U^{A,B}$  are periodic functions of  $x$  and so the band structure is periodic with respect to  $k_x$ , with period  $2\pi$ . On the other hand, the periodicity with respect to  $k_y$  is lost, as can be seen, for



example, in Fig. 4 where the band structure of the one-dimensional model  $\mathbf{k} = (0, 0)$  ( $\Gamma$  point) and  $\mathbf{k} = (0, \pi)$  (Y point) and the band structure between  $\mathbf{k} = (0, -2\pi)$  and  $\mathbf{k} = (0, -\pi)$  (Y point) are plotted for anisotropy  $\alpha_D = 12$  respectively with a solid and dashed curve. Note that the two branches, differing by a reciprocal lattice vector of the two-dimensional vortex lattice  $\mathbf{Q} = (0, -2\pi)$ , cross at the Y point and at non-symmetry points. These crossings become avoided when the non-translational invariance of the full two-dimensional Bogoliubov-de Gennes Hamiltonian (2) is taken into account, but for large enough anisotropy, the resulting gaps can be extremely small. Also, these crossings and the changes they induce in the density of states occur at finite energies and are not too crucial in the understanding of the nature of the low-energy quasiparticle spectrum.

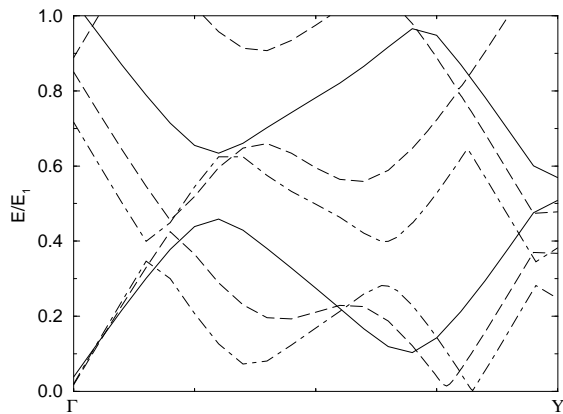


FIG. 6. Band structure of the two-dimensional linearized Bogoliubov-de Gennes equation for a square lattice with anisotropy ratio  $\alpha_D = v_F/v_\Delta = 8, 15, 35$  (solid, dashed and dot-dashed respectively) along the  $\Gamma Y$  direction. Only positive energy bands are plotted for clarity and negative energy bands can be obtained through particle-hole symmetry. The gaps at the  $\Gamma$  point are fictitious, and are due to the chosen lattice discretization scheme (Wilson fermions) of the Hamiltonian. In the  $\alpha_D = 15$  case, only the two lowest bands are plotted, while all the bands with energy  $E < \hbar v_F/d$  are plotted for  $\alpha_D = 8$  and 12. Energies are in units of  $E_1 = \hbar v_F/d$ .

In Fig. 5 we have plotted the one-dimensional band structure for a square vortex lattice with anisotropy ratio  $\alpha_D = 8, 15, 35$  along the  $\Gamma Y$  axes. This plot should be compared to the two-dimensional energy bands calculated in the same direction in the Brillouin zone and plotted in Fig. 6, previously published in<sup>7</sup>. The small gaps at the  $\Gamma$  point in Fig. 6 are fictitious and are due to the choice of real-space discretization (Wilson fermions<sup>20</sup>) of the linearized Bogoliubov-de Gennes equation in two dimensions. In one dimension, we use a different approach (staggered fermions<sup>21</sup>) which preserves the Dirac node at the  $\Gamma$  point in the discretized equations, described in more detail in Appendix II. Similarly to what we ob-

served for the two-dimensional Hamiltonian (2), for large enough anisotropy, the energy spectrum shows new low-energy states around a wavevector close to the Y point. As we mentioned before, the degeneracies observed at the Y point are split as soon as one introduces the non-translational invariance of the Bogoliubov-de Gennes operator.

The strong dependence of the minimum (away from the  $\Gamma$  point) of the lowest-energy band along the  $\Gamma Y$  direction (closest to the Y point) on the anisotropy  $\alpha_D$  is plotted in Fig. 7, along with the asymptotic expression computed in the previous section (the pre-exponential factor has been fitted to the one-dimensional numerical data) and the same data from a fully two-dimensional calculation for values of  $\alpha_D \leq 15$ . The accuracy of the asymptotic expression is remarkably good even for relatively small values of  $\alpha_D$  and the two-dimensional data points are certainly consistent with the one-dimensional approximation.

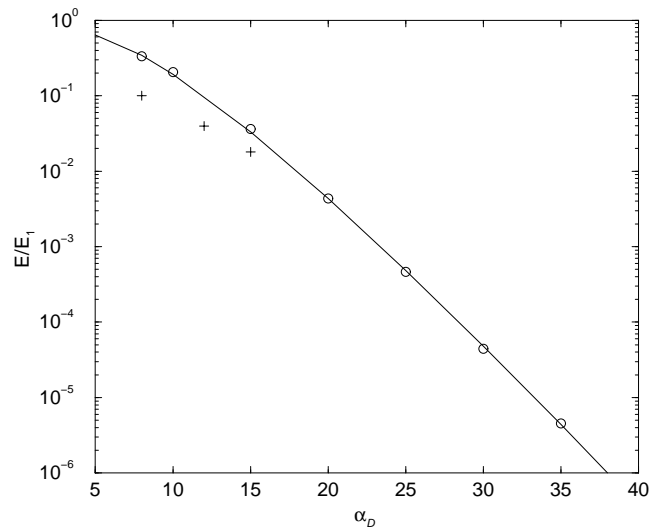


FIG. 7. Energy of the minimum of the positive lowest-energy band (away from the  $\Gamma$  point) along  $\Gamma Y$  as a function of anisotropy  $\alpha_D$ . The circles ( $\circ$ ) represent the results of the one-dimensional model while the pluses ( $+$ ) represent the two-dimensional one. The solid curve is the asymptotic expression calculated in Sect. III, with the pre-exponential factor fitted to the one-dimensional numerical data. Energies are in units of  $E_1 = \hbar v_F/d$ .

We have also computed the band structure in the  $\Gamma X$  direction and studied its dependence on the anisotropy ratio  $\alpha_D$ . Even for relatively modest values of the anisotropy, the lowest energy band is very well approximated by the tight-binding expression

$$\mathcal{E}(k_x) = \Delta E_{\Gamma X} \sin \frac{k_x}{2}, \quad (25)$$

as outlined in the previous section. In Fig. 8, the band structure of the one-dimensional model is plotted for anisotropy  $\alpha_D = 4$ , and it is indistinguishable from the tight-binding expression above. We have computed nu-

merically  $\Delta E_{\Gamma X}$  over a wide range of  $\alpha_D$  and the results are shown in Fig. 9. The solid curve is the exponential behavior computed in Sect. III. The asymptotic result agrees well with the numerical data for large  $\alpha_D$ .

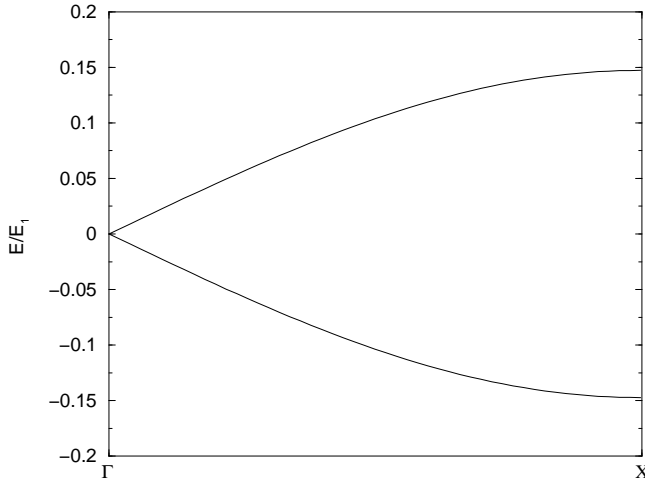


FIG. 8. Band structure for the one-dimensional model with anisotropy  $\alpha_D = v_F/v_j \Delta$  along the  $\Gamma X$  direction. This curve is indistinguishable from the tight-binding expression  $E = 0.15 \sin(k_x/2)$ , plotted on the same scale. Energies are in units of  $E_1 = \hbar v_F/d$ .

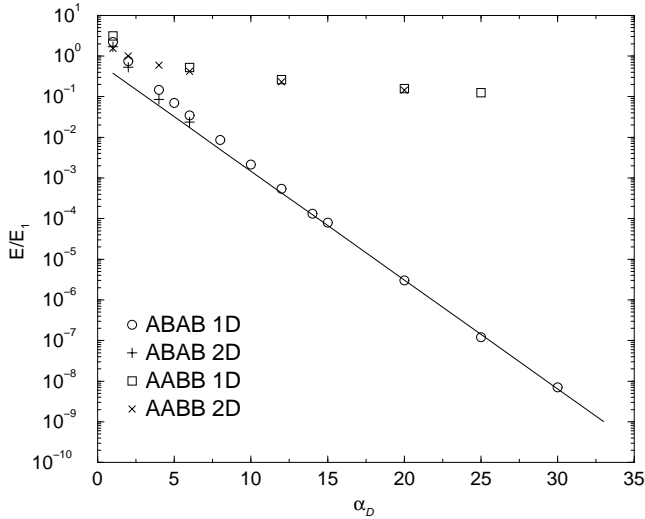


FIG. 9. Width of the lowest-energy band along  $\Gamma X$  as a function of anisotropy  $\alpha_D$ . The solid curve represents the asymptotic expression calculated in Eq. (24), with the pre-exponential factor fitted to the one-dimensional numerical data in the *ABAB* gauge. The circles ( $\circ$ ) are data points obtained by diagonalizing numerically the one-dimensional model in the *ABAB* gauge, while the pluses ( $+$ ) show the bandwidth in the  $\Gamma X$  direction of the two-dimensional Hamiltonian also in the *ABAB* gauge, for moderate anisotropy. The last two data sets plotted show the same energy bandwidth for the one- and two-dimensional model in the *AABB* gauge, plotted with squares ( $\square$ ) and crosses ( $\times$ ), respectively. Energies are in units of  $\hbar v_F/d$ .

## B. Bravais vortex lattice: *AABB* gauge

Let us turn to the numerical diagonalization of the Bogoliubov–de Gennes Hamiltonian for a square vortex lattice in the *AABB* singular gauge. Although it is still a Bravais lattice, the unit cell includes four vortices, as shown in Fig. 2 and it is a  $1 \times 2$  rectangle, in dimensionless units. The coordinates of the high-symmetry points in the first Brillouin zone are therefore  $\mathbf{k} = (0, 0)$  ( $\Gamma$  point),  $\mathbf{k} = (\pi, 0)$  ( $X$  point) and  $\mathbf{k} = (0, \pi/2)$  ( $L$  point). As we discussed in the previous section, we do not expect to find any exponentially small features in the energy band structures for large values of the anisotropy ratio  $\alpha_D$  in this singular gauge.

The different nature of the low-energy states in the two singular gauges can be observed in Fig. 9 where we plot the bandwidth of the lowest  $\Gamma X$  energy band ( $\Delta E_{\Gamma X}$ , as defined in equation (23) in the previous section). Notice the qualitatively different behavior in the two singular gauges we considered. While the bandwidth in the *ABAB* gauge follows very closely the asymptotic exponential dependence on the anisotropy  $\alpha_D$ , the same energy scale in the *AABB* gauge decays in a much slower fashion and does not seem to reach an exponential decay in the anisotropy range considered. In both cases, the one- and two-dimensional calculations agree reasonably well with each other.

We have studied both the one- and two-dimensional Hamiltonians in the *AABB* gauge. Even though the energy bands cannot be computed (even just in the asymptotic limit of large anisotropy) by a simple approach as in the *ABAB* case, the one-dimensional model gives some information about the more involved two-dimensional Hamiltonian. In particular, the one-dimensional calculation of energy bands in the region of the Brillouin zone close to the  $\Gamma$  point is in reasonable agreement with the two-dimensional band structure. More generally, the translational invariance in the direction of smearing of the bands in the  $\Gamma L$  direction — differing by a reciprocal lattice vector  $\mathbf{Q} = (0, -\pi)$  — can cross at the  $L$  point and at non-symmetry points. These crossings, just like in the *ABAB* gauge, become avoided when the translational invariance is broken, as in the two-dimensional case. Unlike in the *ABAB* gauge, the magnitude of the resulting energy gaps does not become exponentially small as we increase the anisotropy ratio. This makes the one-dimensional model not as useful for quantitative calculations of properties of the full two-dimensional Bogoliubov–de Gennes Hamiltonian as in the *ABAB* singular gauge.

The one- and two-dimensional band structures are plotted in Figs. 10 and 11. The energy bands are computed in the  $\Gamma X$  and  $\Gamma L$  directions for anisotropies  $\alpha_D = 12$  and 20. Although the one-dimensional model fails to reproduce all the details of the two-dimensional band

structure away from the  $\Gamma$  point even for relatively large values of the anisotropy, the one-dimensional bands allow to sketch the qualitative behavior of the two-dimensional ones, once the band crossings become avoided. Finally, notice that, while in the  $ABAB$  gauge there was a minimum developing in the lowest energy band already for  $\alpha_D = 8$ , in the  $AABB$  gauge the anisotropy ratio has to be much larger ( $\alpha_D = 20$ ) before we start finding an inflection in the lowest energy band for both the one- and two-dimensional Bogoliubov-de Gennes operators.

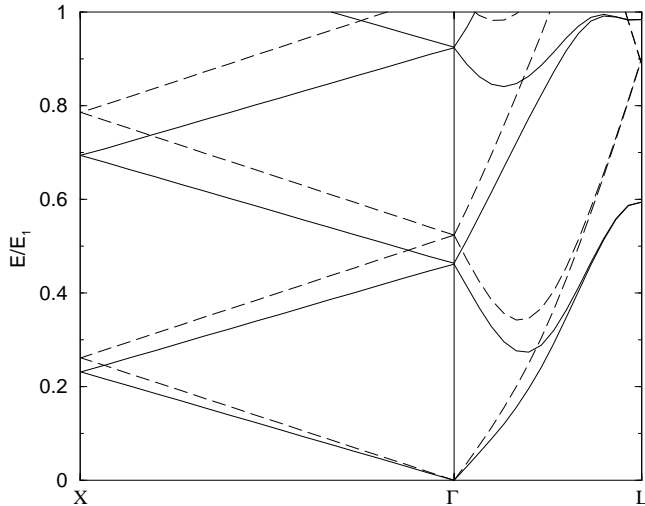


FIG. 10. Band structure for a square vortex lattice in the  $AABB$  singular gauge with  $\alpha_D = v_F/v_\Delta = 12$ . The solid line is the spectrum of the two-dimensional Bogoliubov-de Gennes equation, while the dashed line represents the one-dimensional model. Only positive energy bands are plotted for clarity, negative energy ones can be obtained by particle hole symmetry. Energies are in units of  $E_1 = \hbar v_F/d$ .

In conclusion, even though the band structures in the  $ABAB$  and  $AABB$  gauges are qualitatively similar close to the center of the Brillouin zone, they differ significantly near the edges of the Brillouin zone. While in the  $ABAB$  case all relevant energy scales depend exponentially on the anisotropy ratio  $\alpha_D$ , the same is not true for the  $AABB$  gauge. This behavior is well understood in terms of the simplified one-dimensional model in both gauges, for large values of the anisotropy ratio  $\alpha_D$ .

### C. Non-Bravais vortex lattice

The Bravais lattice nature of the vortex lattices we considered so far ensures the gaplessness of the spectrum at the center of the Brillouin zone<sup>7</sup>. In the  $ABAB$  singular gauge, we can consider a unit cell with two vortices again, but relax the constraint that they sit equidistantly from each other, along the diagonal — *i.e.* the magnitude of  $\mathbf{R}_0$ , as defined in Fig. 1, does not need to be equal to  $\sqrt{2}d/4$ . Let us assume that the two sublattices  $A$  and  $B$  are still square lattices with spacing  $d$ ,

but let us consider, for concreteness, the case where the distance between nearest  $A$  and  $B$  vortices is  $(2\sqrt{2}/5)d$ , which corresponds to vortex coordinates in the unit cell of  $(\pm 1/5, \pm 1/5)$  in dimensionless units. We can use the one-dimensional potentials computed in equations (14) and (15) with  $x_v = 1/5$  to determine the one-dimensional band structure. The energy bands along the  $-Y$  to  $Y$  direction for anisotropy ratios  $\alpha_D = 1$  and 8 are plotted in Figs. 12 and 13, respectively. First of all, we notice that the  $k_x \rightarrow -k_x$  and  $k_y \rightarrow -k_y$  symmetries of the energy spectrum are broken. Fig. 13 exemplifies how the one-dimensional very effectively captures the qualitative features of the two-dimensional band structure also for a non-Bravais lattice in the large anisotropy limit for the same reasons discussed above in the Bravais lattice case.

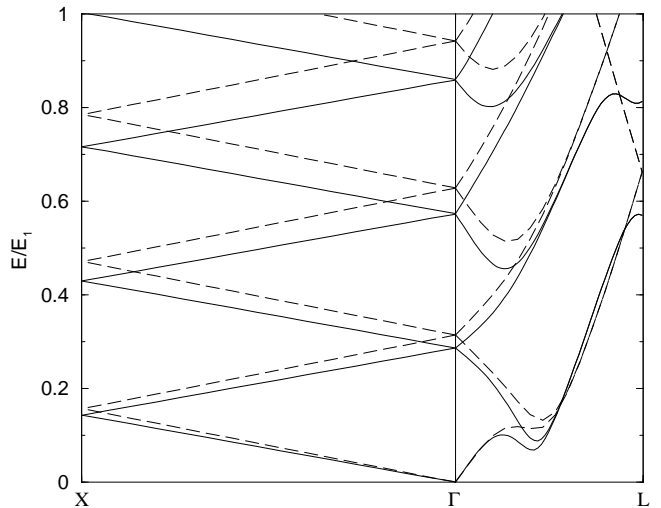


FIG. 11. Band structure for a square vortex lattice in the  $AABB$  singular gauge with  $\alpha_D = v_F/v_\Delta = 20$ . The solid line is the spectrum of the two-dimensional Bogoliubov-de Gennes equation, while the dashed line represents the one-dimensional model. Only positive energy bands are plotted for clarity, negative energy ones can be obtained by particle hole symmetry. Energies are in units of  $E_1 = \hbar v_F/d$ .

We want to emphasize here that, unlike for a Bravais lattice of vortices, the energy spectrum here is gapped. These gaps were discussed in a perturbation theory framework in<sup>7</sup>. What is interesting to note is that the evaluation of these gaps in the one-dimensional model is very consistent with the two-dimensional calculation, even though the handling of the discretization of the linearized Bogoliubov-de Gennes equation is different in the one- and two-dimensional case, as is explained in more detail in Appendix B.

## V. CONCLUSIONS

We have studied the large Fermi-velocity anisotropy  $\alpha_D = v_F/v_\Delta$  limit of the quasiparticle spectrum of a  $d$ -wave superconductor in the mixed state. The vortex geometry we considered is that of a square vortex lattice rotated by  $45^\circ$  from the anisotropy axes. The original linearized Bogoliubov–de Gennes equation was mapped onto a Dirac Hamiltonian in an effective periodic vector and scalar potential using the Franz–Tešanović gauge transformation. We have studied the dependence of the energy spectrum on the choice of such singular gauge transformation. Physically, one might expect the gauge choice not to matter. However, although the Bogoliubov–de Gennes operator considered in this paper is indeed gauge invariant away from the vortices, the singularity at the vortex site introduces boundary conditions that break the invariance of the energy spectrum on the choice of singular gauge.

In the large anisotropy limit, we have solved a one-dimensional variant of the Franz–Tešanović model obtained by smearing the vortices in the “hard” direction. We computed the one-dimensional potentials associated with two different choices of singular gauges in the case of a Bravais square vortex lattice. In one case (the *ABAB* gauge), we found that the low-energy localized states around each vortex type (*A* or *B*) in the one-dimensional potential wells are physically separated. The model can therefore be solved in the WKB approximation and several features of the energy band structure are shown to depend exponentially on the anisotropy ratio  $\alpha_D$ . We compared the computed energy spectrum to the results of a numerical diagonalization of the Hamiltonian (10). In both cases we found that both the minima of the lowest energy-band in the  $\Gamma Y$  direction and the bandwidth of the lowest energy-band in the  $\Gamma X$  direction decay exponentially to zero as a function of the anisotropy  $\alpha_D$ . The asymptotic calculation agrees very well with the numerical results.

Different results are obtained in the *AABB* gauge. In this case, the low-energy states localized around the vortices of different types are not spatially separated. This results in a finite overlap integral for any value of the anisotropy and, therefore, no exponentially small features in the band structure. The one- and two-dimensional numerical spectra in this gauge are not as similar as in the *ABAB* gauge, but one can still extract information like degeneracies or other global properties of the two-dimensional band structure from the one-dimensional calculations. Of course, the detailed spectra will not be equal even in the asymptotic large  $\alpha_D$  limit.

Finally, we have distorted the square vortex lattice in the *ABAB* gauge into a non-Bravais vortex lattice. Again, we find good agreement between the one- and two-dimensional calculations of the energy spectra. In particular, we find a gap in the lowest energy band close to the  $\Gamma$  point (exactly at the center of the Brillouin zone

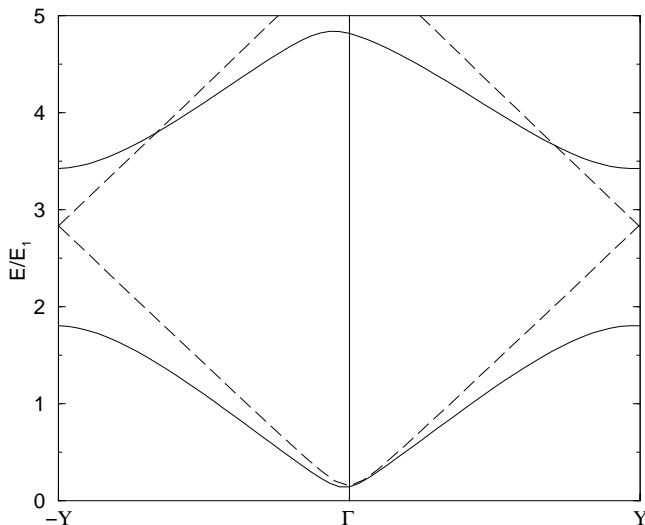


FIG. 12. Band structure for a non-Bravais square vortex lattice in the *ABAB* singular gauge from  $-Y$  to  $Y$  with  $\alpha_D = v_F/v_\Delta = 1$  and vortex coordinates in the unit cell  $(\pm 1/5, \pm 1/5)$ . The solid line is the spectrum of the two-dimensional Bogoliubov–de Gennes equation, while the dashed line represents the one-dimensional model. Only positive energy bands are plotted for clarity, negative energy ones can be obtained by particle hole symmetry. Energies are in units of  $E_1 = \hbar v_F/d$ .

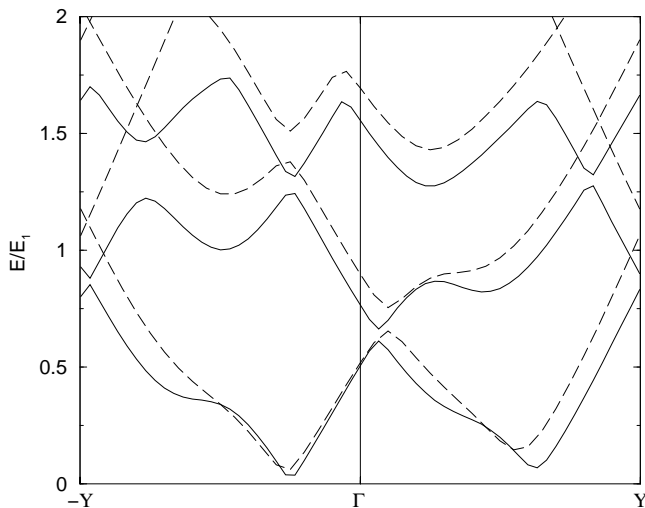


FIG. 13. Band structure for a non-Bravais square vortex lattice in the *ABAB* singular gauge from  $-Y$  to  $Y$  with  $\alpha_D = v_F/v_\Delta = 8$  and vortex coordinates in the unit cell  $(\pm 1/5, \pm 1/5)$ . The solid line is the spectrum of the two-dimensional Bogoliubov–de Gennes equation, while the dashed line represents the one-dimensional model. Only positive energy bands are plotted for clarity, negative energy ones can be obtained by particle hole symmetry. Energies are in units of  $E_1 = \hbar v_F/d$ .

only in the  $\alpha_D = 1$  case, otherwise the  $k_x \rightarrow -k_x$  and  $k_y \rightarrow -k_y$  symmetry of the energy bands is broken) in both numerical calculations.

## VI. ACKNOWLEDGEMENT

The authors are grateful for helpful discussions with S. Simon, M. Hermele, Z. Tešanović, M. Franz, A. Vishwanath, and E. Demler. This work was supported in part by NSF grant DMR-99-81283.

## APPENDIX A: WKB APPROXIMATION FOR THE ONE-DIMENSIONAL MODEL

We want to find the eigenfunctions for a given energy  $E$  of the one-dimensional model in the WKB approximation and derive the appropriate Bohr-Sommerfeld quantization condition. Starting from the one-dimensional Hamiltonian (10), let us define the potentials  $\Phi^A(x) \equiv k_y + U^A(x)$  and  $\Phi^B(x) \equiv -k_y + U^B(x)$  to simplify notations. If we fix the energy  $E$ , we need to find a solution to the system of differential equations

$$\begin{cases} \Phi^A(x)u(x) + \left(\frac{1}{i\alpha_D}\partial_x + \frac{1}{\alpha_D}k_x\right)v(x) = Eu(x) \\ \left(\frac{1}{i\alpha_D}\partial_x + \frac{1}{\alpha_D}k_x\right)u(x) + \Phi^B(x)v(x) = Ev(x). \end{cases} \quad (\text{A1})$$

$$\begin{aligned} u(x) &\sim \left(\frac{E-\Phi^B}{E-\Phi^A}\right)^{1/4} e^{\pm ik_x x} e^{\pm i\alpha_D \int^x dx' \sqrt{(E-\Phi^A(x'))(E-\Phi^B(x'))}} \\ v(x) &\sim \left(\frac{E-\Phi^A}{E-\Phi^B}\right)^{1/4} e^{\pm ik_x x} e^{\pm i\alpha_D \int^x dx' \sqrt{(E-\Phi^A(x'))(E-\Phi^B(x'))}}. \end{aligned} \quad (4)$$

Obviously, these oscillating expressions are correct in the classically allowed regions, while the exponential factors become real in the classically forbidden regions.

## APPENDIX II: NUMERICAL IMPLEMENTATION OF THE ONE-DIMENSIONAL MODEL

To diagonalize the Hamiltonian (10) we have used a real-space representation to take advantage of fast sparse-matrix diagonalization algorithms and to control the smoothing of vortex cores over a finite region of space, which cannot be avoided in a momentum-space representation. The main drawback of discretizing a Dirac-type Hamiltonian in real space is the appearance of the ‘‘Fermion doubling problem’’ (see<sup>21</sup> for a thorough discussion of possible ways of discretizing a Dirac Hamiltonian). The real-space representation of a Dirac Hamiltonian leads to the introduction of  $2^D - 1$  spurious large-wavevector, low-energy modes (additional Fermions, hence the name), where  $D$  is the dimensionality of the system. In our case, the system being one dimensional, there is only one spurious mode, which we

The derivation of the WKB form of the wavefunctions proceeds along standard lines (see for example<sup>22</sup>). Substituting the expansion

$$\begin{aligned} u(x) &= e^{i\alpha_D \sum_{n=0}^{\infty} S_n(x)\alpha_D^{-n}} \\ v(x) &= e^{i\alpha_D \sum_{n=0}^{\infty} T_n(x)\alpha_D^{-n}} \end{aligned} \quad (\text{A2})$$

in the previous system of equations, to find the asymptotic behavior of the wavefunctions for large  $\alpha_D$ . Expanding and equating order by order in  $\alpha_D$  in equation (A1), we can calculate the first two terms in the series (A2), namely  $S_{0,1}(x)$  and  $T_{0,1}(x)$ . These are the leading terms in the expansion for large  $\alpha_D$  and the truncation of the series (A2) to this order is the WKB approximation. In particular,  $S_0(x)$  and  $T_0(x)$  turn out to be

$$S_0(x) = T_0(x) = \pm \int^x dx' \sqrt{(E - \Phi^A(x'))(E - \Phi^B(x'))} \quad (\text{A3})$$

which gives the leading exponential behavior and is the key expression for the Bohr-Sommerfeld quantization formula. Every other term in the series expansion leads to algebraic corrections, which we have not taken into account in this work. For completeness, we state the expression of the WKB wavefunctions, including the algebraic prefactor:

can eliminate using the staggered-fermion approach<sup>21</sup>. If we discretize the vortex lattice unit cell with a mesh of size  $h = 1/(N - 1)$  and index the resulting mesh with an integer  $n$  ranging from  $-N/2$  to  $N/2$  so that  $x = n/N$ , we can place a single-component Fermi field  $\xi(n)$  on each site. To identify a single two-component Dirac field, we can decompose the mesh into an even and an odd sublattice and define

$$\begin{aligned} V(n) &= \xi(n), \quad n \text{ even} \\ W(n) &= \xi(n), \quad n \text{ odd}. \end{aligned} \quad (1)$$

The staggered fermion method avoids the Fermion doubling problem by doubling the size of the unit cell in real space, thus halving the size of the Brillouin zone (and overall number of degrees of freedom). Note that the relevant unit cell here is unrelated to the vortex lattice unit cell, it is simply the unit element of the mesh with which we discretize the continuum equations. Defining the function

$$G(n) = \begin{cases} U^A(n) + k_y, & n \text{ even} \\ U^B(n) - k_y, & n \text{ odd} \end{cases} \quad (2)$$

the discretized eigenvalue problem takes the form

$$\frac{1}{i\alpha_D} \frac{\xi(n+1) - \xi(n-1)}{2h} + G(n)\xi(n) + \frac{1}{\alpha_D} k_x \frac{\xi(n+1) + \xi(n-1)}{2} = E\xi(n) \quad (3)$$

and the correct continuum limit is achieved by letting  $h \rightarrow 0$ , without any further caveats. An important advantage of staggered fermions over Wilson fermions<sup>20</sup> (which we used previously<sup>7</sup>) is that Wilson approach breaks the chiral symmetry of the translationally invariant Hamiltonian, introducing a  $k$ -dependent mass term to lift the spurious modes at the edges of the mesh Brillouin zone to high energy. By explicitly breaking the chiral symmetry, fictitious gaps can and do appear in the energy spectrum at the center of the vortex lattice Brillouin zone thus making it difficult to perform a precise study of almost dispersionless bands, which is one of the goals of the present work. In principle, these gaps could be eliminated to arbitrary precision by carefully tuning suitable counterterms but the procedure (having to be performed numerically) is slow and not very accurate. The staggered fermion approach bypasses all these difficulties by preserving explicitly the chiral symmetry of the one-dimensional Hamiltonian in the lattice representation, if there was one initially in the continuum representation.

---

<sup>1</sup> P. G. de Gennes, *Superconductivity of Metals and Alloys* (Addison-Wesley, Reading, MA, 1989).

<sup>2</sup> L. P. Gor'kov and J. R. Schrieffer, Phys. Rev. Lett. **80**, 3360 (1998).

<sup>3</sup> P. W. Anderson, cond-mat/9812063 (1998).

<sup>4</sup> A. S. Mel'nikov, J. Phys. Cond. Matt. **11**, 4219 (1999).

<sup>5</sup> M. Franz and Z. Tešanović, Phys. Rev. Lett. **84**, 554 (2000).

<sup>6</sup> S. H. Simon and P. A. Lee, Phys. Rev. Lett. **78**, 1548 (1997).

<sup>7</sup> Luca Marinelli, B. I. Halperin, and S. H. Simon, Phys. Rev. B **62**, 3488 (2000).

<sup>8</sup> Daniel Knapp, Catherine Kallin, and A. J. Berlinsky, cond-mat/0011053 (2000).

<sup>9</sup> May Chiao, P. Lambert, R. W. Hill, Christian Lupien, R. Gagnon, Louis Taillefer, and P. Fournier, Phys. Rev. B **62**, 3554 (2000).

<sup>10</sup> J. Mesot, M. R. Norman, H. Ding, M. Randeria, J. C. Campuzano, A. Paramekanti, H. M. Fretwell, A. Kaminski, T. Takeuchi, T. Yokoya, T. Sato, T. Takahashi, T. Mochiku, and K. Kadowaki, Phys. Rev. Lett. **83**, 840 (1999).

<sup>11</sup> O. Vafek, A. Melikyan, and Z. Tešanović, cond-mat/0104516 v2 (2001).

<sup>12</sup> O. Vafek, A. Melikyan, M. Franz, and Z. Tešanović, Phys. Rev. B **63**, 134509 (2001).

<sup>13</sup> G. E. Volovik, JETP Lett. **58**, 469 (1993).

<sup>14</sup> N. B. Kopnin and G. E. Volovik, JETP Lett. **64**, 690 (1996).

<sup>15</sup> G. E. Volovik, JETP Lett. **65**, 491 (1997).

<sup>16</sup> G. E. Volovik and N. B. Kopnin, Phys. Rev. Lett. **78**, 5028 (1997).

<sup>17</sup> B. Revaz, J.-Y. Genoud, A. Junod, K. Neumaier, A. Erb, and E. Walker, Phys. Rev. Lett. **80**, 3364 (1998).

<sup>18</sup> May Chiao, R. W. Hill, Christian Lupien, Bojana Popić, Robert Gagnon, and Louis Taillefer, Phys. Rev. Lett. **82**, 2943 (1999).

<sup>19</sup> Ashvin Vishwanath, cond-mat/0104213 (2001).

<sup>20</sup> K. G. Wilson, in *New Phenomena in Subnuclear Physics*, edited by A. Zichichi (Plenum, New York, 1975), p. 13.

<sup>21</sup> J. B. Kogut, Rev. Mod. Phys. **55**, 775 (1983).

<sup>22</sup> Carl M. Bender and Steven A. Orszag, *Advanced Mathematical Methods for Scientists and Engineers* (McGraw-Hill, New York, NY, 1978).